Optimal Air Gap Length Design in Powder Core Inductors

This article has been accepted for publication in IEEE Transactions on Magnetics. This is the author's version which has not been fully edited and content may change prior to final publication. Citation information: DOI 10.1109/TMAG.2023.3289391

Optimal Air Gap Length Design in Powder Core Inductors

Luigi Solimene, *Student Member, IEEE*, Davide Cittanti, *Member, IEEE*, Fabio Mandrile, *Member, IEEE*, Salvatore Musumeci, *Member, IEEE*, and Radu Bojoi, *Fellow, IEEE*
Politecnico di Torino, Department of Energy "Galileo Ferraris", Turin, Italy, luigi.solimene@polito.it

The main requirements of magnetic components for power electronics applications are high power density and low power losses, driven by the need for more compact and more efficient power converters. Metal powder materials are a common choice for high-power and high-frequency inductors subject to a large magnetic field bias, since they feature high saturation flux density and low magnetic permeability (i.e., a "distributed" air gap), allowing for the adoption of un-gapped cores. Despite this, under high values of magnetomotive force (i.e., deep core magnetic saturation), the insertion of a concentrated air gap can lead to higher core inductance factor values with respect to an un-gapped configuration. In this context, this paper proposes a straightforward procedure to maximize the inductance factor of metal powder magnetic cores by identifying the optimal air gap length for a specified design operating point. In particular, the procedure completely relies on information available in the core manufacturer's datasheet and does not require experimental characterization of the core itself, dramatically simplifying the inductor design procedure. The proposed methodology is theoretically described and then experimentally validated on an XFlux®60 core from Magnetics.

***Index Terms*—metal powder materials, powder cores, magnetic cores, power inductors, air gap, soft saturation, optimization.**

I. Introduction

POWER electronic converters represent a key enabler to the widespread adoption of renewable energy generation, electric transport, and electrified industrial and household appliances. Numerous innovations in the semiconductor industry have led to high power density converters with ever higher switching frequency, up to the MHz range.

Passive components, such as inductors and capacitors, are some of the bulkiest devices in a converter and represent an obstacle to increasing the overall power density. In particular, filter inductors typically operate with a significant magnetic field bias, which represents the main constraint to reducing the component size [1]. As the value of the current through the inductor winding rises, the magnetic field in the core increases as well and the operation of the magnetic material shifts towards the saturation region of the magnetization curve [2]. This implies that the core differential permeability and the component differential inductance drop significantly, and may become unacceptable for the application.

Ferrite cores are widely adopted for filtering applications, in view of their low specific losses and wide avialability. However, these cores are characterized by low saturation flux density and a differential permeability profile featuring a sharp "knee", thus generally requiring a discrete air gap [3].

For these reasons, metal powder cores are increasingly adopted in AC and DC filtering applications, as they allow to significantly improve power density when a large magnetic field bias is required. These cores are manufactured from magnetic alloy grains bound together with an insulating material, creating a distributed air gap and a tunable effective permeability similar to gapped ferrite cores [4], [5]. However, in contrast to ferrite cores, the differential permeability profile of a metal powder core exhibits a gradual (i.e., soft) saturation, with a predictable behavior even at high values of applied magnetic fields [6]. As a consequence of their distributed air gap feature, metal powder cores can typically be adopted in a wide range of applications (i.e., AC and DC current bias) without the need for a concentrated air gap. Nevertheless, when high power density (and thus high magnetomotive force) is required, the addition of a concentrated air gap may improve the inductance factor provided by a given metal powder core [7]. In particular, the optimal length of this air gap is a function of the magnetomotive force set by the application. Fig. 1 qualitatively shows the differential inductance profiles of a powder core inductor for different air gap lengths. As the applied current increases, solutions with a larger concentrated air gap can gradually provide a higher inductance value than solutions without it. Therefore, a maximum inductance profile can be determined and related to an optimal air gap profile as a function of the applied current. According to the design operating point (i.e., nominal current value), the adoption of this optimal air gap length can lead to a significant inductance gain with respect to the un-gapped condition. Remarkably, this solution does not imply specific manufacturing or operational drawbacks if the air gap length is kept within limited values, thus resulting in a pure benefit.

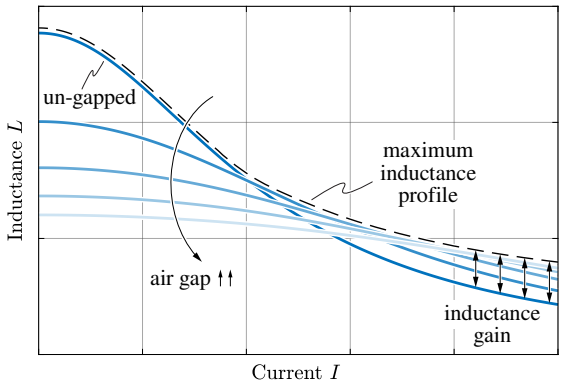

Fig. 1. Qualitative overview of the differential inductance profiles of a metal powder core as functions of the DC-bias current, for different air gap values.

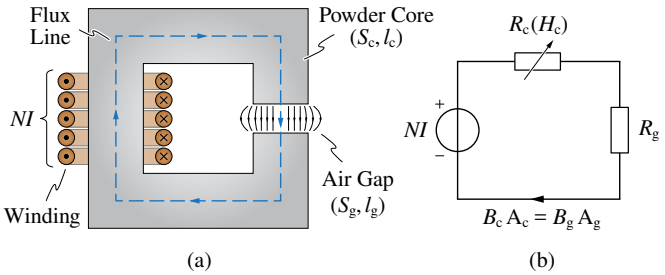

Fig. 2. Considered simplified core model: (a) core and winding dimensions, (b) equivalent circuit representation of the core reluctance.

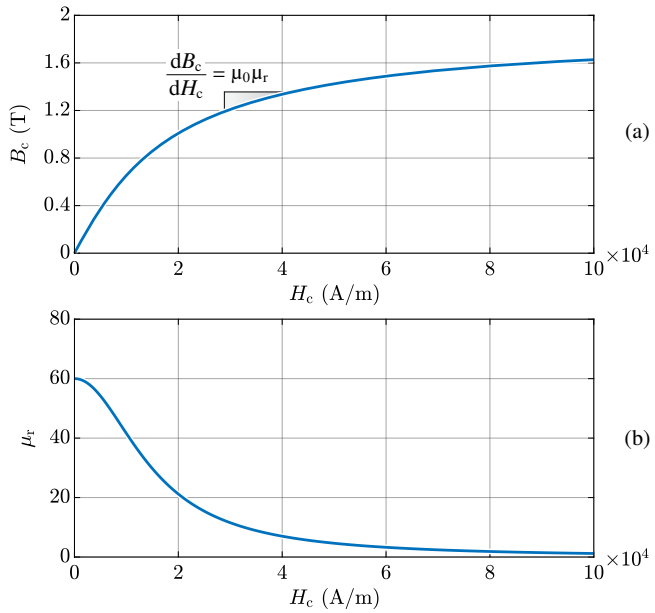

Fig. 3. (a) Magnetization curve of the XFlux®60 from Magnetics and (b) related differential permeability profile as functions of the magnetic field H_c.

Therefore, this paper aims to define and validate a methodology for estimating the optimal air gap length for powder core inductors according to their design specifications. Notably, the proposed method only relies on data available in the manufacturer's datasheet and does not require high computational effort, as the numerical solution of a straightforward magnetic circuit is sufficient to identify the optimal air gap value.

This paper is structured as follows. Section II proposes the methodology for the optimal air gap length computation and directly applies it to a double-E core in XFlux®60 from Magnetics. Section III compares the analytical/numerical estimations with experimental measurements. Finally, Section IV summarizes and concludes this work.

II. Optimal Air Gap Length Computation

Considering a core with an air gap (cf. Fig. 2), the inductance per square turn of a magnetic core, also referred to as inductance factor A_L, can be expressed as

$$A_L = \frac{1}{\mathcal{R}_{tot}}, \tag{1}$$

where the total magnetic reluctance $\mathcal{R}_{tot}$ is defined as

$$\mathcal{R}_{tot}(H_c) = \mathcal{R}_c(H_c) + \mathcal{R}_g = \frac{l_c}{\mu_0\mu_r(H_c)S_c} + \frac{l_g}{\mu_0 S_g}. \tag{2}$$

In (2), μ_0 is the vacuum permeability, H_c, $\mathcal{R}_c$, S_c, l_c and μ_r are the magnetic field, reluctance, cross-section, equivalent path length and relative magnetic permeability of the core, respectively, whereas $\mathcal{R}_g$, S_g and l_g are the reluctance, cross-section and length of the air gap, respectively. In particular, the relative permeability of the magnetic material μ_r is a function of the magnetic field in the core H_c, as reported in Fig. 3, which shows the magnetization curve and the related differential permeability profile of the XFlux®60 metal powder material from Magnetics [8].

The computation of the magnetic field in the core material, generated by the magnetomotive force NI, is determined through the Ampere's law, as

$$H_c(NI, l_g) = \frac{NI - H_g l_g}{l_c}, \tag{3}$$

where H_g is the magnetic field in the air gap. For a given value of NI, adding a concentrated air gap reduces the magnetic field in the core material (i.e., the higher the air gap length, the lower the magnetic field in the core). Therefore, estimating the total reluctance for a gapped core requires the computation of the operating magnetic field in the magnetic material, which is a function of the applied magnetomotive force and the air gap length.

Fig. 4(a) shows the behavior of the core reluctance $\mathcal{R}_c$, air gap reluctance $\mathcal{R}_g$ and total reluctance $\mathcal{R}_{tot}$ of a 6527 double-E (i.e., EE) core in XFlux®60 (cf. Section II-A) as functions of the air gap length l_g at a given magnetomotive force NI. It is clearly observed that, for a given value of NI, an optimal air gap length exists, which minimizes the total reluctance and thus maximizes the inductance factor of a core. In particular, Fig. 4(b) highlights that the optimal air gap length $l_{g,opt}$ increases together with the applied magnetomotive force.

The value of $l_{g,opt}$ that minimizes the total core reluctance can be identified by formally solving the following:

$$\max\left[A_L(NI, l_g)\right] \iff \min\left[\mathcal{R}_{tot}(NI, l_g)\right]. \tag{4}$$

In other words, (4) corresponds to determining the air gap length l_g for each applied magnetomotive force value NI that minimizes the total reluctance of the magnetic circuit, or

$$\left.\frac{d\mathcal{R}_{tot}}{dl_g}\right|_{NI} = 0 \iff \left.\frac{d\mathcal{R}_c}{dl_g}\right|_{NI} = -\left.\frac{d\mathcal{R}_g}{dl_g}\right|_{NI}, \tag{5}$$

which, considering (2) and (3), corresponds to solve

$$\frac{l_c}{\mu_0 S_c}\frac{d}{dl_g}\left(\frac{1}{\mu_r(NI, l_g)}\right) = -\frac{1}{\mu_0}\frac{d}{dl_g}\left(\frac{l_g}{S_g}\right). \tag{6}$$

The sole complexity of the proposed approach, which only requires data provided by the core manufacturer's catalogs (i.e., core geometry, core material magnetization curve), derives from the non-linearity introduced by the magnetic characteristic of the core material. For this reason, (6) cannot be solved analytically, and a numerical (iterative) method must be used instead. In this work, the polarization fixed point method is adopted [9].

This article has been accepted for publication in IEEE Transactions on Magnetics. This is the author's version which has not been fully edited and content may change prior to final publication. Citation information: DOI 10.1109/TMAG.2023.3289391

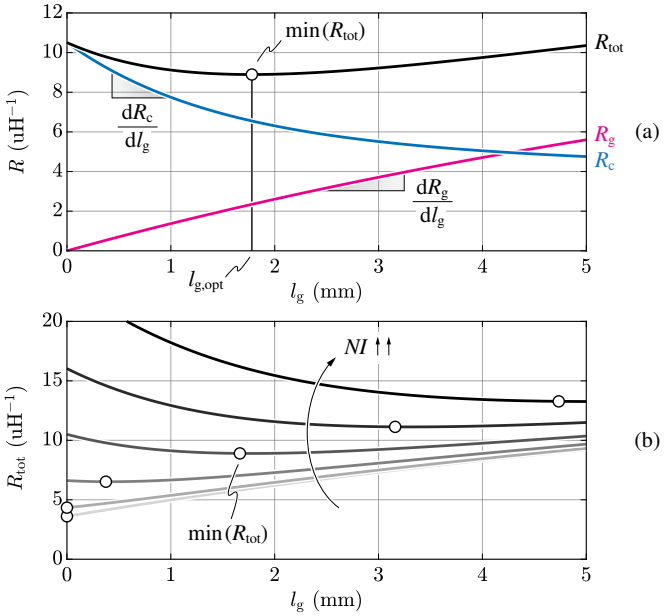

Fig. 4. (a) Core reluctance $\mathcal{R}_{\mathrm{c}}$, air gap reluctance $\mathcal{R}_{\mathrm{g}}$ and total reluctance $\mathcal{R}_{\mathrm{tot}}$ profiles of a 6527 EE core in XFlux®60 as functions of the air gap length l_{g} at a given magnetomotive force NI. The minimum value of $\mathcal{R}_{\mathrm{tot}}$ is indicated by ○. (b) Total reluctance $\mathcal{R}_{\mathrm{tot}}$ profiles as functions of the air gap length l_{g} and increasing magnetomotive force values NI. The minimum reluctance points (○) identify the optimal air gap profile $l_{\mathrm{g,opt}}(NI)$.

A. Case Study: 6527 EE Core in XFlux®60

The proposed optimal air gap length computation method is here applied to a 6527 double-E (i.e., EE) core in XFlux®60 from Magnetics, schematically illustrated in Fig. 6(a) (cf. Section III). The geometrical dimensions l_{c} and S_{c} adopted for the computation of the ferromagnetic path reluctance $\mathcal{R}_{\mathrm{c}}$ in (6) are respectively the effective magnetic path length and cross-section provided in the core datasheet. For the computation of the air gap reluctance $\mathcal{R}_{\mathrm{g}}$, the air gap cross-section S_{g} is defined to account for the flux fringing effect as [10]

$$S_{\mathrm{g}} = (a + l_{\mathrm{g}}) \cdot (b + l_{\mathrm{g}}), \tag{7}$$

where a and b are the two dimensions of the core central column cross-section, as illustrated in Fig. 6(a). It is worth noting that (7) is here adopted to achieve a good trade-off between accuracy and overall complexity, however more accurate S_{g} estimation methods can be found in literature [11].

The solution of (6) for different values of NI allows to identify the optimal air gap length profile for the selected core, as reported in Fig. 5(a). This profile maximizes the core inductance factor for every operating point, providing increasing benefits with respect to an un-gapped core at higher magnetomotive force values, as shown in Fig. 5(b). In fact, the addition of a suitable discrete air gap helps to reduce the operating flux density and thus to maintain a higher differential permeability at high magnetomotive force, as illustrated in Fig. 5(c) and Fig. 5(d), respectively.

III. Experimental Validation

The optimal air gap length identification procedure outlined in Section II is here verified experimentally by assessing the

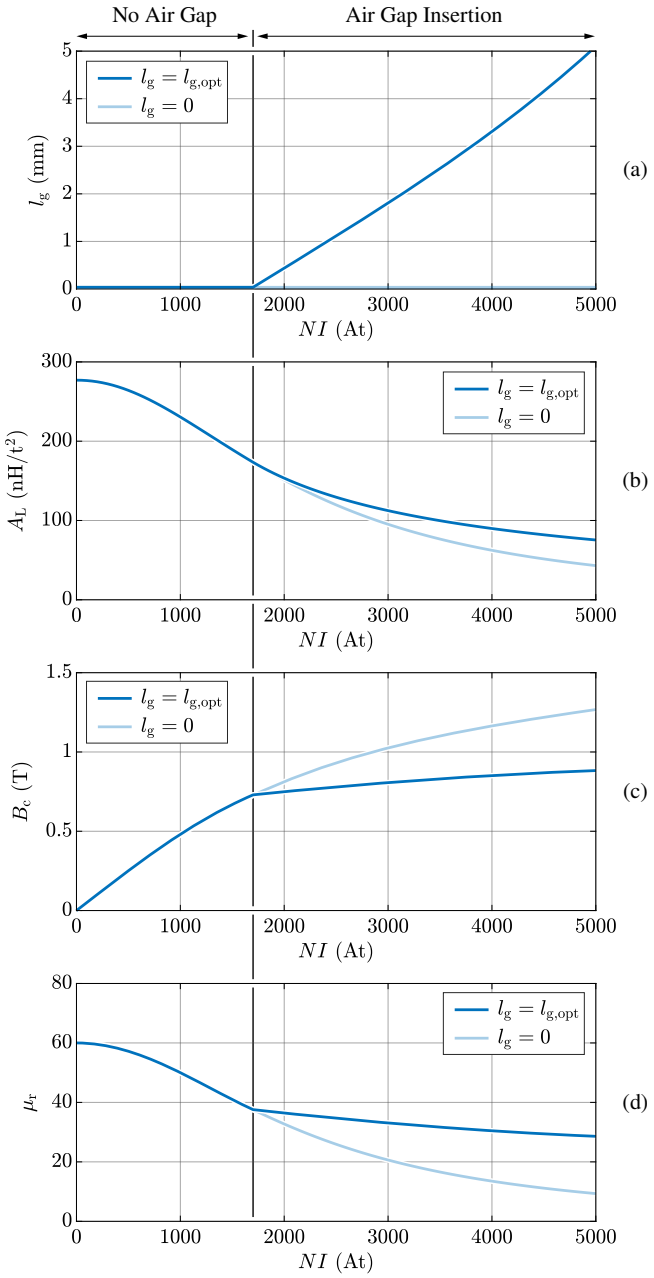

Fig. 5. Results of the optimal air gap computation procedure applied to a 6527 EE core in XFlux®60 and comparison with the corresponding un-gapped core. (a) optimal air gap l_{g}, (b) core inductance factor A_{L}, (c) core magnetic flux density B_{c}, and (d) core relative permeability μ_{r} as functions of the applied magnetomotive force NI.

differential inductance of a purposely constructed inductor sample as a function of the applied magnetomotive force. The inductor sample is illustrated in Fig. 6(b) and consists of two stacked sets of 6527 EE cores, a coil former and two windings wound around the central core column, namely a measuring winding ($N_1 = 50$ turns) and a magnetizing winding ($N_2 = 150$ turns).

The experimental setup consists of two identical inductor samples (i.e., the devices under test, DUTs), a regulated DC power supply, a high-precision LCR meter, and a set of decoupling inductors, as shown in Fig. 7. The two DUTs

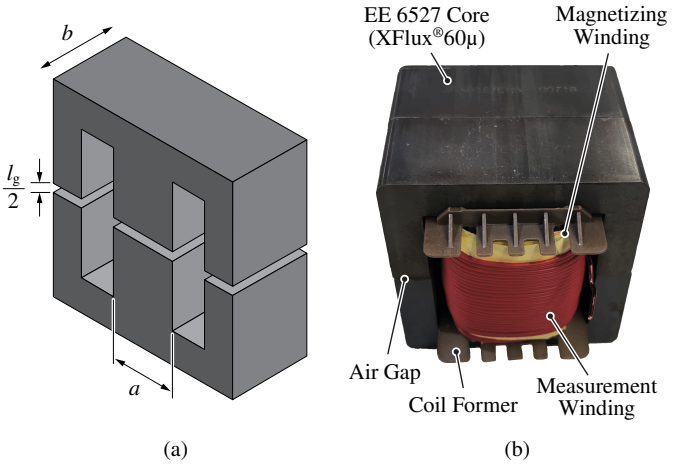

Fig. 6. (a) Drawing of the considered 6527 EE core, highlighting the required dimensions to calculate the air gap cross-section S_g according to (7). (b) Photo of the sample used for the experimental tests (i.e., device under test, DUT).

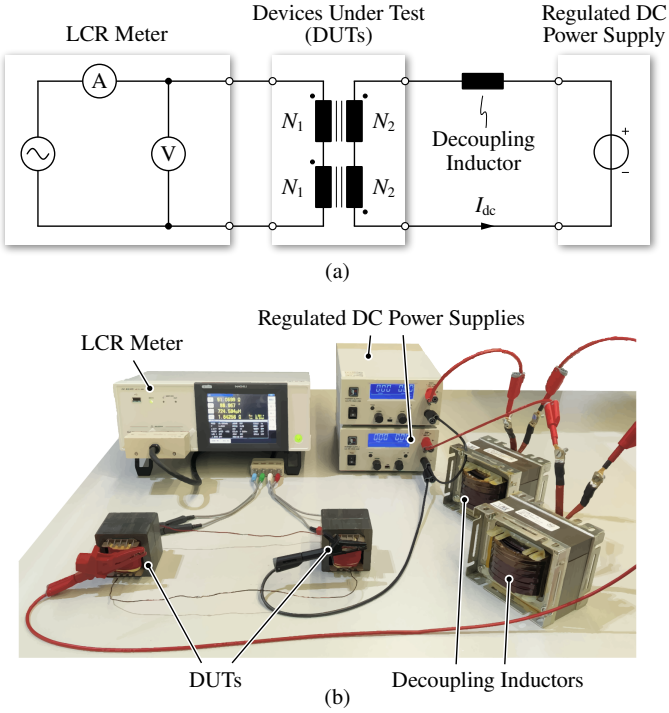

Fig. 7. (a) Schematic of the experimental setup to measure the differential inductance profile as a function of the magnetomotive force. (b) Photo of the experimental setup.

are connected in series at the primary side (measurement windings) and in anti-series at the secondary side (magnetizing windings), so that the measuring circuit (i.e., the LCR meter) is theoretically decoupled from the magnetizing circuit. The magnetizing circuit is powered by a regulated power supply unit delivering up to 20 A. Under these conditions, the core can be tested with a magnetomotive force up to $NI = 3000$ At. The measurement winding is connected to a high-precision LCR meter (i.e., Hioki IM3536), which performs an accurate impedance measurement by imposing a 5 kHz small-signal sinusoidal voltage and measuring the current flowing through the circuit. The DUT differential inductance value is directly obtained from the impedance information, assuming an RL (series) equivalent circuit. Besides the anti-series connection of the magnetizing windings, generating balanced and opposite induced voltages, to further enhance the decoupling between the measuring and magnetizing circuits, two high-value (i.e., 6 mH) decoupling inductors are added in series to the DC power supply.

Exploiting the setup of Fig. 7, different sets of measurements are performed at various air gap lengths (i.e., namely, 0, 0.5, 1.0, 1.5 and 2 mm) and magnetomotive force values (i.e., varied continuously between 0 and 3000 At). A maximum air gap length of 2 mm is considered, since higher values would be difficult to ensure with proper accuracy and could also result in a poor estimation of the flux fringing effects.

First, the inductance factor profile resulting from the measurement in un-gapped core conditions (i.e., $l_g = 0$) is compared with the curve provided by the manufacturer in the core datasheet, to verify the accuracy of the measurement setup. The total inductance measured by the LCR meter is divided by two (i.e., two DUTs in series) and then divided by N_1^2, obtaining the A_L value of a single inductor. Since the core datasheet considers a single core pair, the A_L obtained experimentally is further divided by two and the comparative results are shown in Fig. 8. It is observed that the measured A_L is coherent with the data provided in the core datasheet, which is specified with a tolerance of $\pm 8\,\%$ around the nominal value.

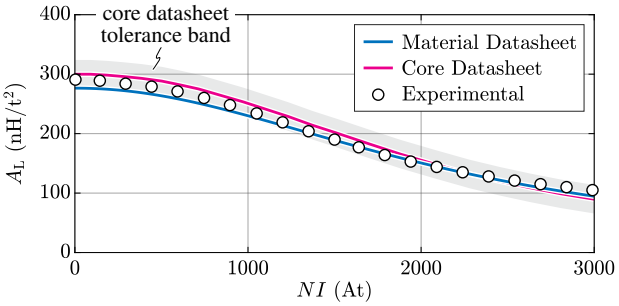

Fig. 8. Measured inductance factor profile of a 6527 EE core in XFlux®60, compared with the data provided by the manufacturer. The blue curve represents the A_L estimation based on the material datasheet and the core dimensions, whereas the pink curve directly reports the A_L value found in the core datasheet. The $\pm 8\,\%$ tolerance band is highlighted in grey.

Additionally, Fig. 8 displays the estimated A_L profile obtained exploiting the material characteristics and the core dimensions according to (1) and (2). The main source of the discrepancy between the estimated (blue) and provided (pink) A_L profiles is to be attributed to the low relative permeability of the core, which leads to a distributed fringing field in the air around the inductor that increases the overall inductance factor and is unaccounted for in the theoretical calculation of the core reluctance $\mathcal{R}_c$.

As a second validation step, to verify the optimal air gap length computation procedure, the same inductance profile characterization test is performed for different air gap length values. The results are illustrated in Fig. 9(a). It is worth noting that, in contrast to the previously reported A_L profiles, Fig. 9(a) shows the A_L value of the complete DUT (i.e.,

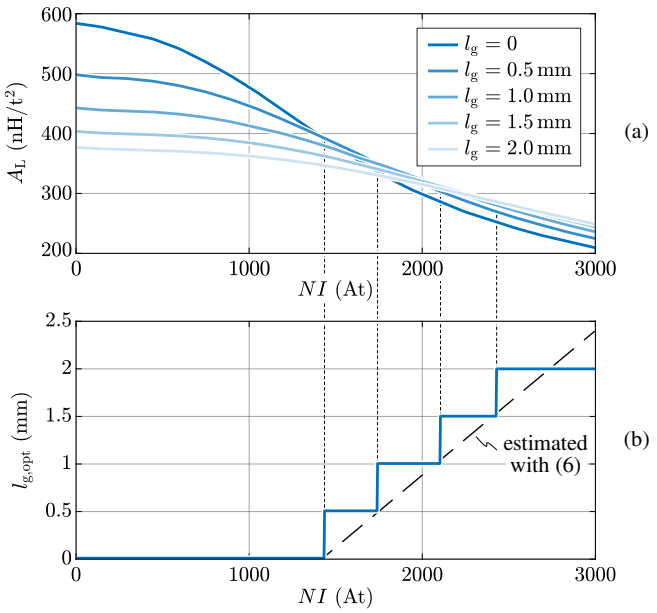

Fig. 9. (a) Measured inductance factor A_L profiles of a single DUT for different air gap length l_g values and (b) optimal air gap length $l_{g,opt}$ as function of the applied magnetomotive force NI. The value of $l_{g,opt}$ estimated with (6) is indicated with a dashed line in (b).

made up by two EE core pairs, cf. Fig. 6(b)). This is because, once the air gap is introduced, the measured inductance can no longer be linearly scaled to estimate the A_L of a single core pair, due to the non-linear air gap cross section definition (7). In particular, for a given value of l_g, two paralleled core pairs feature less S_g (i.e., less fringing field) that two times the S_g of a single core pair, due to the ratio between l_g and the core column perimeter being lower in the former case. It is observed that the un-gapped core features the highest A_L profile up to a magnetomotive force $NI \approx 1400\,\mathrm{At}$, after which the addition of a discrete air gap becomes beneficial and translates in a $\approx 20\,\%$ A_L enhancement at $NI = 3000\,\mathrm{At}$. This is highlighted in Fig. 9(b), where the optimal air gap value among 0, 0.5, 1.0, 1.5 and $2\,\mathrm{mm}$ is identified by selecting the maximum $A_L(l_g)$ profile as function of NI. The highly discretized optimal air gap value obtained experimentally is also compared to the one estimated according to (6), exploiting the material characteristics and the core geometrical dimensions. Remarkably, the agreement between the two curves highlights that the optimal air gap length of a powder core inductor can be calculated with good accuracy even when relying only on the material characteristics and core dimensions provided in the manufacturer's datasheet. This allows to avoid a dedicated core characterization procedure, thus dramatically simplifying the inductor design process.

IV. Conclusions

Metal powder cores are widely adopted in the design of power inductors operating with a DC or low-frequency AC bias field. These cores feature high saturation flux density, relatively low specific losses and distributed air gap. This characteristic, in particular, allows the core to sustain a high magnetomotive force (i.e., a high current bias) in un-gapped configurations without being subject to a large and sharp inductance drop, as opposed to ferrite cores. Despite this, adding a suitable concentrated air gap under high magnetomotive force values may enable higher core inductance factors, allowing to maximize the performance of a given core over a broader range of magnetic field bias and thus maximizing the inductor power density.

To this end, the present paper has proposed a procedure to identify the optimal air gap length that maximizes the inductance factor of a given metal powder core as a function of the magnetomotive force set by the application. The proposed methodology is based on the iterative numerical solution of a straightforward non-linear reluctance model and completely relies on information directly available in the core manufacturer's datasheet, requiring no experimental characterization.

In particular, the air gap optimization procedure has been verified with experimental measurements, determining the inductance factor of a 6527 double-E core in XFlux®60 (from Magnetics) with different air gap length values and under a wide range of applied magnetomotive force values. The results have demonstrated excellent agreement between the numerical estimation of the optimal air gap profile and the experimental data, verifying that the adoption of a suitable discrete air gap can effectively maximize the inductance factor of a metal powder core at high magnetomotive force values.

V. Acknowledgment

This work has been partially funded by the project "ISoREC - Innovative Solutions for Renewables in Energy Communities" funded by the Italian MUR PRIN, Bando 2020 - grant 202054TZLF.

References

[1] J. Kaiser and T. Dürbaum, "An Overview of Saturable Inductors: Applications to Power Supplies," *IEEE Transactions on Power Electronics*, vol. 36, no. 9, pp. 10 766–10 775, Sep. 2021.

[2] J. D. Pollock, W. Lundquist, and C. R. Sullivan, "Predicting Inductance Roll-Off with DC Excitations," in *IEEE Energy Conversion Congress and Exposition*, Sep. 2011, pp. 2139–2145.

[3] T. Ge, K. Ngo, J. Moss, and M. Lim, "Gap design for nonlinear ferrite cores to maximize inductance," in *IEEE Energy Conversion Congress and Exposition (ECCE)*, Sep. 2014, pp. 5237–5242.

[4] F. Fiorillo, G. Bertotti, C. Appino, and M. Pasquale, *Soft Magnetic Materials*. Hoboken, NJ, USA: John Wiley & Sons, Inc., Dec. 1999.

[5] W. G. Hurley, M. C. Duffy, J. Acero, Z. Ouyang, and J. Zhang, "17 - Magnetic Circuit Design for Power Electronics," in *Power Electronics Handbook (Fourth Edition)*, M. H. Rashid, Ed. Butterworth-Heinemann, Jan. 2018, pp. 571–589.

[6] J. Imaoka, K. Okamoto, M. Shoyama, Y. Ishikura, M. Noah, and M. Yamamoto, "Modeling, Magnetic Design, Simulation Methods, and Experimental Evaluation of Various Powder Cores Used in Power Converters Considering Their DC Superimposition Characteristics," *IEEE Transactions on Power Electronics*, vol. 34, no. 9, pp. 9033–9051, Sep. 2019.

[7] J. Imaoka, W. Yu-Hsin, K. Shigematsu, M. Noah, M. Yamamoto, and W. Martinez, "A Magnetic Design Method for Powder Core Inductor with Concentrated Airgap Considering DC Superposition Characteristics Used for High Current Applications," in *European Conference on Power Electronics and Applications (EPE - ECCE Europe)*, Sep. 2021.

[8] "Magnetics - XFlux Cores." [Online]. Available: https://www.mag-inc.com/Products/Powder-Cores/XFlux-Cores

[9] M. Chiampi, D. Chiarabaglio, and M. Repetto, "An accurate investigation on numerical methods for nonlinear magnetic field problems," *Journal of Magnetism and Magnetic Materials*, vol. 133, no. 1, pp. 591–595, May 1994.

[10] N. Mohan, T. M. Undeland, and W. P. Robbins, *Power electronics: converters, applications, and design*, 3rd ed. Hoboken, NJ: John Wiley & Sons, 2003.

[11] J. Mühlethaler, "Modeling and Multi-Objective Optimization of Inductive Power Components," Ph.D. dissertation, ETH Zurich, 2012.